Photophysical Behavior and Assignment of the Low-Energy Chlorophyll States in the CP43 Proximal Antenna Protein of Higher Plant Photosystem II†

Joseph L. Hughes,*,‡ Rafael Picorel,§,|| Michael Seibert,§ and Elmars Krausz‡

Research School of Chemistry, The Australian National University, Canberra, ACT 0200, Australia, National Renewable Energy Laboratory, Golden, Colorado 80401-3393, and Estación Experimental de Aula Dei, CSIC, Apdo. 202, 50080 Zaragoza, Spain

Received July 19, 2006; Revised Manuscript Received August 15, 2006

ABSTRACT: We have employed absorption, circular dichroism (CD), and persistent spectral hole-burning measurements at 1.7 K to study the photoconversion properties and exciton coupling of low-energy chlorophylls (Chls) in the CP43 proximal antenna light-harvesting subunit of photosystem II (PSII) isolated from spinach. These ∼683 nm states act as traps for excitation energy in isolated CP43. They "bleach" at 683 nm upon illumination and photoconvert to a form absorbing in the range ∼660−680 nm. We present new data that show the changes in the CD spectrum due to the photoconversion process. These changes occur in parallel with those in absorption, providing evidence that the feature undergoing the apparent bleach is a component of a weakly exciton-coupled system. From our photoconversion difference spectra, we assign four states in the Chl long-wavelength region of CP43, two of which are the known trap states and are both highly localized on single Chls. The other two states are associated with weak exciton coupling (maximally ∼50 cm^{-1}) to one of these traps. We propose a mechanism for photoconversion that involves Chl−protein hydrogen bonding. New hole-burning data are presented that indicate this mechanism is distinct to that for narrow-band spectral hole burning in CP43. We discuss the photophysical behavior of the Chl trap states in *isolated* CP43 compared to their behavior in *intact* PSII preparations. The latter represent a more intact, physiological complex, and we find no clear evidence that they exhibit the photoconversion process reported here.

Proximal Antenna Subunits of Photosystem II. Photosystem II (PSII)[1] is a Chl-containing, transmembrane, multisubunit protein complex responsible for photocatalyzing water oxidation and plastoquinone reduction. The Chl-containing proximal antenna proteins CP43 and CP47 mediate the transfer of excitation energy from the main light-harvesting antenna assemblies of PSII to the reaction center, where light-induced charge separation and subsequent redox chemistry occur. By appropriate detergent treatments, PSII can be prepared as either membrane-bound or detergent-solubilized forms (*1*−*4*). The minimal PSII preparation capable of oxygen evolution is a PSII core complex, containing the CP43 and CP47 antenna subunits and the D1 and D2 proteins binding the redox components of the reaction center, as well as the cytochrome b_{559} subunit, the Mn-containing oxygen-evolving system, and other smaller proteins. CP43 and CP47 are closely associated with the D1-D2 reaction center proteins (*5*−*10*). As well as a light-harvesting functionality, the proximal antennae may have significance in stabilizing the oxygen-evolving site (*11*).

Spectroscopic studies of PSII to assess structure and function properties have received significant attention in the past 2 decades (see refs *12*−*18* and references cited therein). Recent medium-resolution X-ray crystallographic studies (*5*−*10*) have identified the position and relative orientations of Chl pigments in a cyanobacterial PSII core complex. In core complexes of *Thermosynechococcus elongatus*, 13 and 16 regions of electron density have been assigned to Chl *a* in CP43 and CP47, respectively, while 14 Chl *a* have been identified in CP43 of *Thermosynechococcus vulcanus* (*6*). Chl *a* in the proximal antennae are quite well described as being in layers on the stromal and lumenal sides of the membrane (*5*−*9*, *19*). Natively, PSII occurs as a homodimer where the two monomers are related by a pseudo-C2 rotation axis located perpendicular to the membrane plane. The close association of the CP47 subunit with the D1-D2 proteins is near the interface of the two monomers in the homodimer. CP43 has a more peripheral location in PSII than CP47 and is known (*11*, *20*) to be much easier to remove from a PSII core than CP47.

In plants, CP43 may be involved with energy transfer from both the minor antenna protein, CP26, and the main light-harvesting protein, LHCII, to the reaction center (*21*, *22*). CP47 apparently plays a greater structural role in the dimerization of a PSII core while potentially acting as a

† M.S. and R.P. appreciate support from the Energy Biosciences Division, Basic Energy Sciences, Office of Science, U.S. Department of Energy. R.P. also acknowledges the MYCT in Spain (Grant BMC2005-07422-C02-01).

* Corresponding author. Telephone: +61-2-6125-3577. Fax: +61-2-6125-0750. E-mail: hughes@rsc.anu.edu.au.

‡ The Australian National University.

§ National Renewable Energy Laboratory.

|| Estación Experimental de Aula Dei, CSIC.

[1] Abbreviations: Chl, chlorophyll; PSII, photosystem II; cyt b_{559}, the cytochrome b_{559} subunit of photosystem II; CD, circular dichroism; T − S, triplet minus singlet absorption difference; FLN, fluorescence line narrowing; fwhm, full width at half-maximum height; NPHB, nonphotochemical spectral hole burning; ZPH, zero phonon hole; PSBH, phonon sideband hole; TLS, two-level system.

10.1021/bi0614683 CCC: $33.50
Published on Web 09/16/2006

conduit for energy transfer from the minor antennae proteins CP29 and CP24 (*21*, *22*). By isolating the Chl-containing protein subunits of PSII and studying them spectroscopically, various groups have successfully elucidated particular energy-transfer pathways and their time scales. However, there are key aspects of the energy-transfer pathway that remain controversial, in particular the final step of excitation transfer from the proximal antennae to the reaction center Chls (*13*−*15*, *18*, *23*−*40*). This step is emerging as a significant feature of models for energy equilibration and charge separation in PSII (*13*, *15*, *23*, *24*, *26*, *27*, *34*−*36*, *39*−*44*), and it is therefore important to characterize and understand the behavior of the lowest energy Chl states in the proximal antenna proteins.

The Trap Chlorophylls in Isolated CP43. There is a well-known (*20*, *38*, *45*−*47*) long-wavelength feature at ∼683 nm in the absorption spectrum of isolated CP43, and the Chl states associated with this shoulder are known to trap excitation energy in the isolated subunit (*38*, *45*, *47*). The long-wavelength states in CP43 have commonly been thought to extend to lower energy than that of the primary electron donor in PSII (∼680−683 nm) and therefore act as a trap for excitation at low temperatures in oxygen-evolving PSII. A large body of work on isolated CP43/CP47 antenna subunits, D1-D2-cyt b_{559}, and CP47-D1-D2-cyt b_{559} preparations has been modeled to suggest that the "linker" Chls in PSII are in equilibrium with the reaction center Chl and are not those Chls that act as traps in the isolated CP43/CP47 subunits (*13*, *15*, *23*, *24*, *26*, *27*, *34*−*36*, *39*−*43*). In the reversible radical pair model for primary charge separation in PSII there is a rapid equilibration of excitation between the proximal antennae and the PSII reaction center.

Our assignment (*14*, *28*−*32*, *48*, *49*) of the linker Chls at low temperature (<10 K) in oxygen-evolving PSII preparations is different to what has often been assumed and/or modeled at higher temperatures. We have shown (*31*, *50*) via illumination-induced electrochromism at 1.7 K in dark-adapted spinach PSII core complexes that excitation in the wavelength region 695−730 nm leads to primary charge separation and subsequent formation of the $S_1Q_A^-$ configuration. With illumination in the 690−700 nm range, Q_A^- formation occurs with high quantum efficiency (1−0.1) in a large fraction of centers. The photoconversion behavior is essentially the same as that seen with green light (*31*). In conjunction with our spectral hole-burning data (*14*, *29*, *32*), this indicates that the long-wavelength trap states in isolated CP43 and CP47 act as "linkers" between the proximal antennae and the reaction center Chl in oxygen-evolving PSII at low temperatures. However, they transfer energy at a rate that is competitive with fluorescence lifetimes. Within this assignment, the emitting states in PSII are necessarily the linker Chls (*28*). It is clear that characterization of the behavior of the long-wavelength Chl states in the proximal antennae becomes an important issue for understanding the energy-transfer processes in PSII.

Spectral hole burning by Jankowiak et al. (*45*) at 4.2 K and fluorescence lin narrowing (FLN) at 5 K by Groot et al. (*47*) have shown that in isolated CP43 there exist two long wavelength Chl states that act as traps for excitation energy at low temperatures. The states were labeled A (683.3 nm) and B (683.0 nm) by Jankowiak et al. (*45*), with fwhm ∼120 and ∼45 cm^{-1}, respectively. The B-state was thought to be the primary trap for excitation energy in isolated CP43 and was therefore suggested by Jankowiak et al. (*45*) to be important for transferring excitation energy to the reaction center. The premise for the assignment by Jankowiak et al. (*45*) of the B-state as the primary trap for excitation in CP43 is addressed in the present work. We suggest that both the A- and B-states can be equally effective traps for excitation energy in isolated CP43 and hence equally effective as energy-transfer linkers to the reaction center in more intact PSII preparations.

Jankowiak et al. (*45*) determined that the A- and-B states both undergo persistent nonphotochemical spectral hole burning (NPHB) with comparable efficiencies, on the basis of their contribution to the zero-phonon hole-burning action spectrum and their comparable radiative lifetimes. A narrow "bleach" (∼45 cm^{-1} fwhm) in the absorption difference spectrum that is associated with photoconversion of the B-state is observed following hole burning at wavelengths greater than ∼680 nm (*45*, *46*). The photoconversion of the A-state is less efficient than the B-state and results in a broader (∼120 cm^{-1}) contribution to the absorption difference spectrum (*45*). These absorption changes have been associated with the NPHB process (*45*). We have reported (*46*) that the B-state depletion could be induced via white-light illumination, suggesting that it is distinct from the narrow-band hole-burning process. In this work we particularly address the distinction between NPHB and photoconversion processes, in addition to the efficiencies of photoconversion for the A- and B-states. This distinction is significant, as broad features in NPHB spectra for many Chl−protein systems have often been discussed in terms of the electronic coupling between exciton-coupled chromophores (*51*−*54*).

Exciton Coupling in the Isolated CP43 Subunit. The 77 K triplet-minus-singlet absorption difference (T − S) spectra of Groot et al. (*47*) provide evidence for exciton coupling between the Chls in isolated CP43 associated with the long-wavelength absorption region. T − S spectra are referred to as triplet bottleneck hole-burning spectra by Jankowiak et al. (*45*). The presence of intense features in the circular dichroism (CD) spectrum and an anomalously low Stark effect were both used (*47*) as further evidence for exciton coupling in CP43. Jankowiak et al. (*45*) and Groot et al. (*47*) both suggested that the narrow (B) state is only weakly coupled to other Chl pigments and that the B-state excitation is strongly localized on a single Chl. Jankowiak et al. (*45*) suggested that the A-state is strongly localized on a single Chl located in the other Chl *a* layer (see above) to that in which the B-state Chl resides.

Groot et al. (*47*) have suggested that the broader state in the long-wavelength region is due to several excitonically coupled Chls. This was supported (*38*) by Monte Carlo modeling studies based on the 3.8 Å resolution crystal structure of a PSII core complex (*5*). However, the B-state could not be accounted for, and it was suggested that the origin of the red shift of the B-state may not be excitonic.

One aim of the present study was to investigate the photoconversion properties of long-wavelength Chl pigments in the isolated CP43 subunit with regard to the nature of these long-wavelength states. In our novel approach, we utilize changes in the circular dichroism spectrum accompanying photoconversion of isolated CP43 to clearly

identify the presence of exciton coupling in long-wavelength trap states. By adopting the assignment (*14*, *28*−*32*, *48*, *49*) that the trap Chls in the isolated CP43 subunit become linker Chls in oxygen-evolving PSII at low temperatures, we expect that their photophysical behavior in the assembled system might be significantly different. This possibility is briefly discussed.

METHODS

Biochemical Samples and Optical Spectroscopy. Isolation of CP43 subunits from spinach was performed as described elsewhere (*20*, *45*). All subsequent sample handling was performed under dim green light. For optical spectroscopy, samples were diluted with 40−45% 1:1 ethylene glycol/glycerol glassing agent and placed in an ∼0.2 mm pathlength quartz-windowed cell assembly. This achieved an optical density in the Chl Q_y region of ∼1. The cell assembly was attached to the sample rod and lowered into an Oxford Instruments SM4 cryostat, where cooling to 4 K occurred over a period of ∼40 s. All optical measurements were performed in superfluid liquid helium at 1.7 K. Absorption and circular dichroism measurements were made simultaneously on an instrument constructed in our laboratory that has previously been described (*55*). The same instrument was used for measuring the pre- and postburn absorption spectra for the hole-burning measurements, as well as for the pre- and postillumination absorption spectra for the nonresonantly excited photoconversion measurements. Control absorption measurements were routinely performed to ensure that no net reduction of the integrated absorption associated with Chl had occurred. For all illuminations in this report, minimal permanent depletion of integrated absorption in the Chl Q_y region (<0.5% of the area corresponding to 1 Chl) was observed.

Illumination Sources. Non-wavelength-selective photoconversions (i.e., those not leading to NPHB) were performed with one of three difference excitation sources. The first two used a 150 W halogen lamp passed through a 10 cm water bath and a filter stack. The filter stack was chosen so as to pass either green light (540 nm peak transmission, fwhm ∼50 nm) or orange light (595 nm peak transmission, fwhm ∼50 nm), and both produced ∼4 mW/cm^2 at the sample. The third excitation source was the 488 nm line from a Spectra Physics model 165 Ar* ion laser, focused to ∼0.1−1 J/cm^2 at the sample. The 488 nm line was chosen to avoid NPHB in the Chl pigments while allowing for greater absorbed fluences at the sample.

Spectral holes were burned using a Spectra Physics model 375 dye laser operating with DCM dye, pumped by a Spectra Physics model 171 Ar* ion laser. A three-plate birefringent filter was used for wavelength selection. The line width of the dye laser matched the resolution of the monochromator (∼1.5 cm^{-1}) used for pre- and postburn readout of absorption spectra, as described above. The fluence used for hole burning was 30−50 mW/cm^2.

RESULTS

Photoconversion-Induced CP43 Absorption Changes. Absorption difference spectra of the Chl *a* Q_y region of isolated CP43 at 1.7 K, showing the changes that occur due to illumination with 488 nm light (155 mW/cm^2), are seen in Figure 1. These spectra show the photoconversion of long-wavelength Chl *a* in CP43. The thick trace is the absorption spectrum at 1.7 K prior to any illumination and agrees well with that previously reported at low temperature (*45*−*47*). The absorption depletion near ∼683 nm aligns with the prominent long-wavelength absorption feature. The photoproduct distribution associated with the photoconversion is in the 660−680 nm range, as indicated in Figure 1 by the shaded region. These phenomena are consistent with our previous preliminary report (*46*).

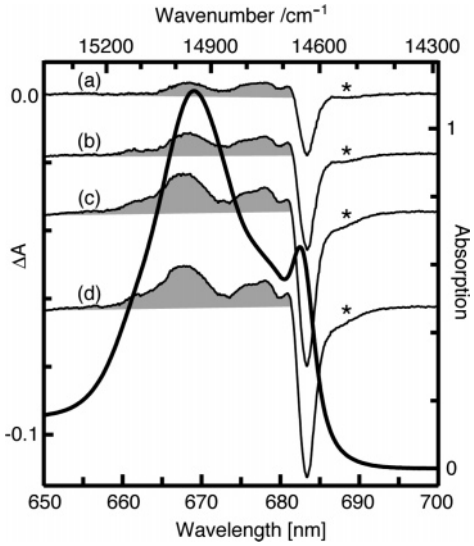

FIGURE 1: Absorption spectrum in the Chl *a* Q_y region at 1.7 K of CP43 isolated from spinach prior to any illumination (thick trace). The thin traces (a−d) are the absorption difference spectra following illumination at 488 nm with 9.3, 27.9, 93, and 139.5 J/cm^2, respectively. The absorption difference spectrum is the absorption spectrum measured after illumination minus that measured before illumination. Traces b−d have been offset for clarity. The shaded region shows the photoproduct distribution associated with the absorption depletion near 683 nm. The asterisk identifies the region where using higher illumination fluences leads to a greater contribution from a broad feature (see text for details).

The photoproduct distribution has broad maxima at ∼668 and ∼677 nm and a minimum at ∼673 nm. There is some finer structure associated with these broad features that we do not discuss in detail. The area of the ∼668 nm feature increases relative to the ∼677 nm feature for difference spectra obtained after illumination with greater fluence (Figure 1). We attribute the ∼668 and ∼677 nm systems to two different photoproduct distributions.

There is a clear negative feature in the difference spectrum at ∼680 nm. There is also a broader negative contribution to the absorption difference spectra at wavelengths longer than ∼686 nm (Figures 1 and 2). Jankowiak et al. (*45*) suggested that the depletion in this region is partly due to aggregation phenomena, based on its dependence on detergent concentration. For the difference spectra obtained with lower fluence (e.g., Figure 1, traces a and b) this feature is easier to identify than in the higher fluence traces (e.g., Figure 1, traces c and d). Further details of this phenomenon are presented in Figure 2.

Absorption difference spectra of the ∼683 nm depletion feature obtained upon illumination with 8.5 J/cm^2 using a lamp plus orange filter stack and with 540 J/cm^2 using the 488 nm line from an Ar* ion laser are shown in Figure 2. In

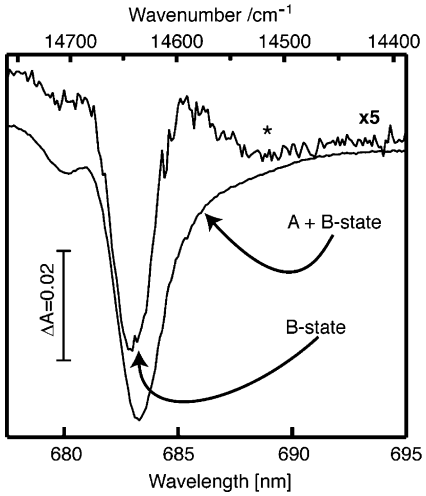

FIGURE 2: Absorption difference spectrum after illumination with 8.5 J/cm^2 using a lamp plus orange filter stack (top trace) and with 540 J/cm^2 using the 488 nm line from an Ar* ion laser (bottom trace). The top trace has been multiplied by a factor of 5. The preillumination absorption spectrum is the same as that shown in Figure 1. At lower fluences the depletion is dominated by a single, sharp feature assigned to the B-state (top trace), while at higher fluences the contribution from the B-state as well as a broad feature assigned to the A-state is apparent (see text for assignment details). The small relatively sharp feature indicated by the asterisk is attributed to aggregation phenomena (see text for details).

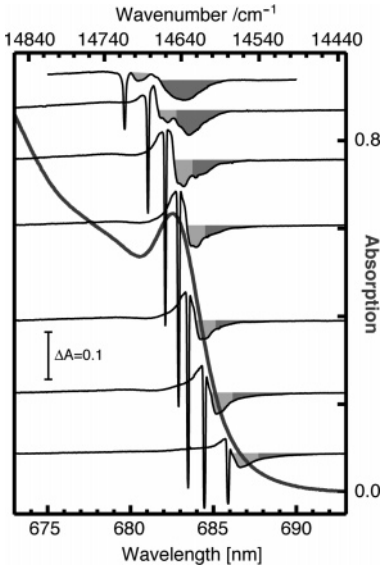

FIGURE 3: Saturated nonphotochemical persistent spectral holes burned at 1.7 K in isolated CP43. The thick gray trace is the preburn absorption spectrum. The sharp negative features are the ZPHs, which are resonant with the laser burn wavelength. The sharp positive features immediately adjacent to the ZPHs are the photoproduct. The light shaded region indicates the pseudo-PSBH, while the dark shaded region indicates the contribution from the non-wavelength-selective photoconversion. The hole-burned spectra, from top to bottom, were obtained after using burn fluences of 24, 27, 18, 9, 9, 18, and 36 J/cm^2, respectively.

each case the preillumination absorption spectrum is the same as that in Figure 1. The top trace (Figure 2) has been multiplied by a factor of 5. For higher fluence illuminations resulting in larger absorption depletion, the peak position in the absorption difference spectrum undergoes a slight red shift from 683.0 to 683.3 nm. In addition, at higher absorbed fluences the spectra show that the depletion at wavelengths longer than ~686 nm is dominated by a contribution from a broader state, as suggested above. Photoconversion of the broader state is less efficient than that of the dominant (narrow) ~683 nm state. The contribution from the broader state is distinct from the changes associated with aggregation phenomena. The bleach due to aggregation phenomena is only evident in difference spectra obtained at fluences less than ~10 J/cm^2 at 488 nm (Figures 1 and 2).

The broadening of the absorption depletion for the high-fluence spectrum compared to the low-fluence spectrum is attributed to photoconversion of the A-state occurring in addition to that of the B-state. The shift of the peak wavelength of the depletion may be due to the contribution from the A-state or to selectivity in the photoconversion process (see Discussion). In 4.2 K hole-burning measurements with excitation at 670 nm using 200 mW/cm^2 for 75 min (900 J/cm^2), Jankowiak et al. (*45*) also reported a broadening of the ~683 nm depletion feature. At the highest illumination fluences we utilized, the area of the depletion at ~683 nm corresponded to ~0.1 Chl. The balance between photoproduct and depletion areas established that there was no significant loss of Chl absorption strength and consequently no permanent Chl oxidation or photodegradation. In the Discussion section we quantify the contributions from the A- and B-states in the absorption spectra.

We estimated the quantum efficiency of photoconversion in a manner analogous to that for hole-burning quantum efficiencies (*14*, *56*) and find that it is initially of the order ~10^{-5}. The quantum efficiency is estimated by the ratio of absorbing centers that have photoconverted, monitored by the depletion area, to the number of absorbed photons. The growth kinetics of photoconversion is dispersive, exhibiting a decreasing efficiency as a function of increasing illumination fluence (data not shown).

In this work we found that the photoconverted state is metastable at 1.7 K, exhibiting <10% decay of the difference spectrum over a period of 1 h. The photoconversion is >95% reversible by thermal cycling to ~70 K for 10 min. Also, the measurement light from the monochromator did not induce any detectable photoconversion of the sample.

Competition between Spectral Hole Burning and Photoconversion. For narrow-band (e.g., laser) excitation that is resonant with the Chl *a* Q_y region of the A- and B-states, spectral hole burning and photoconversion occur concomitantly (*45*, *46*). Spectral hole burning gives rise to a sharp zero-phonon hole (ZPH) that is resonant with the laser burn wavelength (λ_B) and a broader pseudo-phonon sideband hole (pseudo-PSBH) structure to lower energy (*57*−*59*). Hole-burning spectra are the difference of absorption measured after narrow-band illumination minus the absorption spectrum measured before illumination. When the electron−phonon coupling is weak, as for the long-wavelength Chl *a* in CP43 (*45*−*47*), the real PSBH which is situated at higher energy than the ZPH is not apparent.

A survey of saturated persistent nonphotochemical spectral holes (thin traces) burned at 1.7 K in the ~679−686 nm wavelength region of isolated CP43 is shown in Figure 3. The preburn absorption spectrum (thick gray trace) is also presented for comparison. Each hole was burned in a sample that had been annealed to ~100 K for ~10 min. This procedure recovers photoconverted Chl and also fills in any

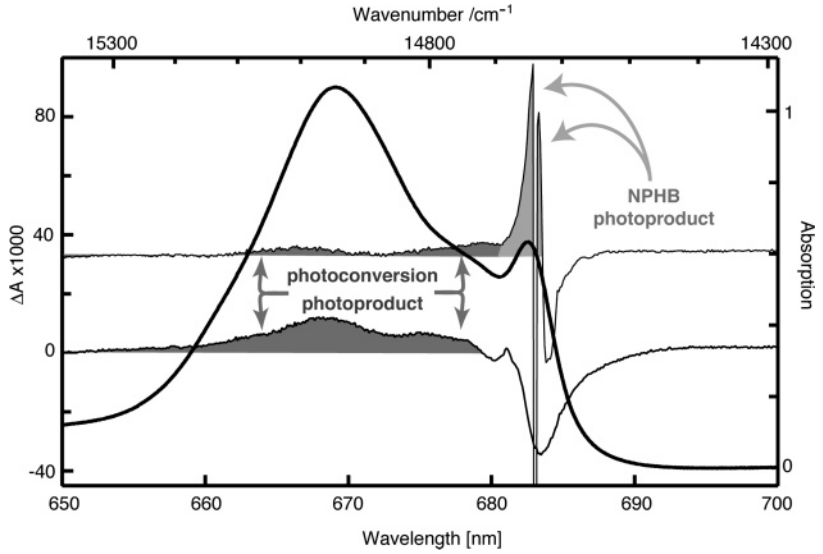

FIGURE 4: Comparison of the non-wavelength-selective photoconversion absorption difference spectra obtained at 1.7 K with 270 J/cm^2 of 488 nm light (900 mW/cm^2, 5 min, bottom thin trace) and a saturated persistent spectral hole burned at 683.0 nm with 9 J/cm^2 also at 1.7 K (150 mW/cm^2, 1 min, top thin trace). The spectral hole was burned after the 488 nm illumination. The absorption spectrum prior to any illuminations is also shown for comparison (thick trace). The dark shaded area indicates photoproduct associated with non-wavelength-selective photoconverison, which is distinct to that associated with narrow-band NPHB (light shaded area). The sharp ZPH has been truncated for clarity, and the NPHB spectrum has been offset for clarity.

spectral holes that had been previously burnt. The hole-burned spectra presented in Figure 3 contain contributions from the non-wavelength-selective process as well as the features associated with NPHB. The hole-burned structure is evident in Figure 3 by the sharp, narrow negative feature (ZPH) and the pseudo-PSBH to lower energy indicated by the lightly shaded region. The darker shaded region indicates the contribution from the non-wavelength-selective photoconversion. The pseudo-PSBH structure exhibits two resolved features found at -15 and -24 cm^{-1} from the ZPH, which has been associated (*46*) with phonon sidebands of the A- and B-states, respectively. A detailed discussion of the pseudo-PSBH structure is beyond the scope of the present report.

For excitation at λ_B <680 nm, in addition to the hole-burning feature, the B-state photoconversion (*45*, *46*) depletion becomes evident and is centered at ~683.2 nm with fwhm ~45−50 cm^{-1} (Figure 3). For excitation at λ_B >680 nm, the B-state photoconversion feature is attenuated, and the spectrum is dominated by features attributable to hole burning. As an example, for excitation at 681.0 nm a ZPH and pseudo-PSBH are observed, but *only* the Chls contributing to the longer wavelength region of the B-state are depleted (Figure 3). This suggests that the dominant process upon direct excitation of the A- and B-states is hole burning, and the non-wavelength-selective photoconversion is less efficient. For hole burning at progressively longer wavelengths, the contribution from the photoconversion feature becomes less evident (dark shaded regions in Figure 3) and lies outside the ~45−50 cm^{-1} width of the B-state feature, consistent with the additional photoconversion arising from the A-state.

Photoproduct Distributions. Immediately adjacent to the resonant ZPH is the hole-burning photoproduct, identified as a relatively sharp positive feature(s) (Figure 3). For holes burned at longer wavelengths (684−686 nm) the photoproduct distribution is predominantly to the blue of the resonant hole, and for holes burned at shorter wavelengths (679−681 nm) it is to the red. For hole burning at intermediate wavelengths (681−684 nm) the photoproduct is distributed approximately equally on either side of the resonant hole. This behavior is characteristic of the NPHB process (*57*, *58*) where absorption associated with a photoproduct lies within the inhomogeneous distribution of the state being burned.

The photoproduct that is associated with the non-wavelength-selective photoconversion lies well outside the inhomogeneous distribution of long-wavelength Chl *a* states but within the Q_y distribution of CP43 Chls (Figures 1, 3, and 4). Figure 4 shows that the photoproduct of this photoconversion (dark shaded region) is clearly distinct from the NPHB photoproduct (light shaded region). The sharp ZPH resonant with the burn wavelength (λ_B = 683 nm) has been truncated in Figure 4. This hole was burned *after* the non-wavelength-selective photoconversion shown in Figure 4 in order to obtain a hole-burning spectrum with minimal contribution from the former process. In this difference spectrum there is minimal further depletion and associated photoproduct due to the non-wavelength-selective photoconversion. The NPHB process dominates features in the low-energy region.

Photoconversion-Induced Circular Dichroism Changes. The non-wavelength-selective depletion feature corresponds well to the strong negative component in the circular dichroism (CD) spectrum. This can be seen in Figure 5 where the absorption and CD spectra of CP43 at 1.7 K are presented (thick traces), as well as the absorption difference spectrum obtained after 540 J/cm^2 illumination at 488 nm (thin trace). The CD spectrum agrees with that previously reported by Groot et al. (*47*) at 77 K. It is interesting to note that the weaker feature identified in the absorption difference spectra at ~680 aligns quite well with the sharp positive CD feature near ~680 nm. The ~683 and ~680 nm features can be assigned as components of an exciton-coupled system and will be considered in more detail below. The majority of

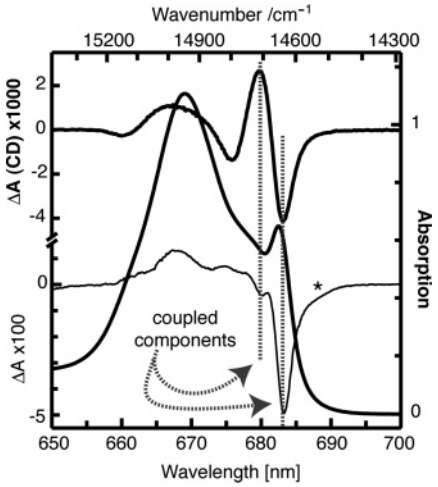

FIGURE 5: Comparison of the 1.7 K CP43 CD spectrum (top section) and photoconversion absorption difference spectra obtained at 1.7 K with 900 mW/cm^2 of 488 nm light for 10 min (bottom section). The dotted vertical gray lines indicate features associated with exciton-coupled components (see text for assignment). The asterisk indicates the contribution from the (broad) A-state.

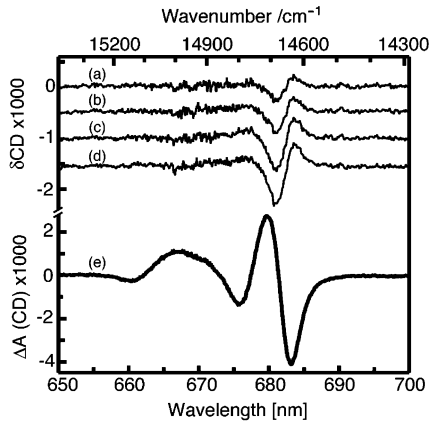

FIGURE 6: Traces a−d present the changes in the 1.7 K CP43 CD spectrum (trace e, thick trace) after illumination with 488 nm light. Traces b−d have been offset for clarity. These spectra were obtained simultaneously with those in Figure 1, and the fluences used are therefore the same. The CD difference spectra are representative of the exciton CD of the coupled system associated with the B-state (see text for details).

the intensity of the strong negative CD feature near 683 nm is associated with the B-state. This is clear from a comparison of the CD spectrum and the non-wavelength-selective absorption difference spectrum in the region of the shoulder associated with the A-state. This assignment of the 683 nm CD feature as mainly associated with the narrow (B) state is consistent with the suggestion by Groot et al. (*47*).

The changes in CD due to photoconversion at 1.7 K occur in parallel with those seen in absorption. Figure 6 shows a fluence dependence of changes observed in the CD spectrum of the Chl *a* Q_y region after photoconversion using 488 nm excitation (thin traces, a−d). The CD spectrum prior to any illuminations is also shown for comparison (thick trace). All CD and absorption spectra were measured simultaneously (see Methods), and the fluence dependence of the CD changes shown in Figure 6 was measured concurrently with that for the absorption changes shown in Figure 1. The CD difference spectrum (δCD in Figure 6) is conservative, with the integrated change in CD being zero. This is consistent with the conservative absorption difference spectrum (see above) showing no Chl *a* oxidation or photodegradation. The δCD spectrum is the change in CD associated with photoconversion and represents the loss of CD of the initial form of the photoconverted pigments. Unlike the absorption difference spectra, there is no evidence for a significant CD associated with the photoproduct.

Monomeric Chl *a* exhibits only a weak negative CD signal in the Q_y region (*60*, *61*), with $\Delta\epsilon = -14$ M^{-1} cm^{-1} at room temperature in ether (*61*). By comparison, $\Delta\epsilon$ (scaled per CP43) at 679.8 and 683.1 nm in Figures 5 and 6) are +2300 and −3500 M^{-1} cm^{-1}, respectively. This is consistent with their assignment to components of a coupled system, as exciton coupling can induce CD far larger than due to monomeric Chl *a* contributions (*62*, *63*). The CD induced by this mechanism is however conservative. Quantification of the features in the CD difference spectra is provided in the Discussion section.

The δCD spectrum is simpler than the CD spectrum and is dominated by changes in the long-wavelength region where the non-wavelength-selective absorption depletion occurs. The positive δCD feature peaking at 683.8 nm can be associated with a loss of exciton CD of the B-state. The (−) exciton CD of the B-state is due to coupling with an exciton partner, which gives rise to the (+) CD peak for this partner at 681.0 nm. The presence of such a B-state partner is indicated by a depletion feature in the absorption difference spectrum of Figure 5 at ∼680 nm. There are clearly features in the CD spectrum of CP43 in the 660−680 nm region which are not represented in the δCD spectrum, and we associate these with other exciton-coupled pigments in CP43 not associated with the states that undergo photoconversion. Overlap of these states with that giving rise to the δCD feature at 681.0 nm may be responsible for the difference in this position and the position of the CD feature at 679.8 nm. A detailed assignment of the long-wavelength states is provided in the Discussion.

DISCUSSION

Assignment of the Long-Wavelength Chl a States in CP43. In this section we consider the assignment of the long-wavelength states in isolated CP43 based on absorption and CD photoconversion difference spectra. The CD spectrum indicates significant exciton coupling among the long-wavelength Chl *a* state(s) [see the Results section and Groot et al. (*47*)], and we use this to guide a global fit to CD difference spectra. Our assignments are then related to those made by Jankowiak et al. (*45*) and Groot et al. (*47*).

A minimal description of the CD difference spectrum requires three Gaussian bands. In particular, one broad band and one sharp band cannot describe the CD difference spectrum. We performed a global fit of the four CD difference spectra in Figure 6, with the positions and widths of the Gaussians used as global parameters. With no constraints imposed in the fit, there is strong correlation between the fwhm, position, and areas of two of the Gaussian bands. Weak correlation was observed between the parameters of the third component and those of the other two Gaussians. The fwhm and area for the two strongly correlated Gaussians were found to be quite similar, as might be

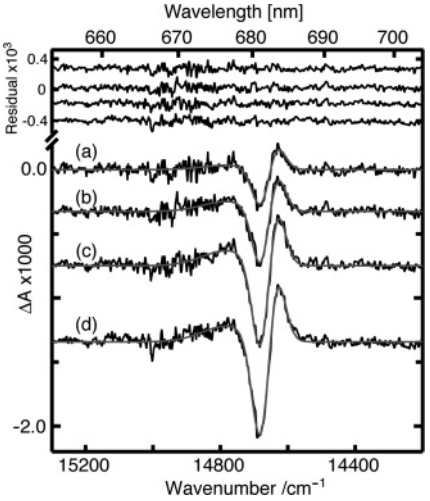

FIGURE 7: The global fit (gray traces) to the CD difference spectra (black traces, a−d) of CP43. The residuals of the fit are presented in the top section. See text for details.

Table 1: Long-Wavelength Chl *a* States in Isolated CP43

band	position (nm)	position (cm^{-1})	fwhm (cm^{-1})
(1) B-state	682.7 ± 2.5	14650 ± 55	70 ± 15
(2) B-state exciton partner	681.7 ± 2.1	14670 ± 45	70 ± 15
(3) B-state exciton partner	676.6 ± 0.5	14780 ± 10	180 ± 15
(4) A-state	683.0 ± 0.3	14640 ± 7	170 ± 30

expected if they represent components of an exciton-coupled system. As a first-order approximation we therefore constrained these two widths to be the same and described the area of the second Gaussian as $area_2 = f(area_1)$, where f was used as a global parameter in the fit. The requirement of $area_1 = area_2$ resulted in a poor fit.

The constrained global fit to the CD difference spectrum and the associated residuals are shown in Figure 7, while the fit parameters are given in Table 1. The fit places the two correlated states identified as (1) and (2) in Table 1 at 14650 ± 55 cm^{-1} (682.7 ± 2.5 nm) and 14670 ± 45 cm^{-1} (681.7 ± 2.1 nm) with fwhm = 70 ± 15 cm^{-1}. A sharp feature peaking near ∼680 nm was also found in the absorption difference spectrum (Figure 5), which is consistent with these two sharp features, (1) and (2), being components of an exciton-coupled system. The relatively large errors are due to the considerable correlation between the two sharp components, as discussed above.

From the error values it may appear that both bands 1 and 2 can be at the same energy at the same time and therefore cancel. However, from the data this is clearly not the case, and this feature of the error values is a consequence of the correlation between the two bands. In the fits, band 1 is always at lower energy than band 2. If the band positions vary within the errors from the fit values (682.7 ± 2.5 and 681.7 ± 2.1), they do so in a correlated fashion, and the widths vary accordingly (70 ± 15 cm^{-1}) to produce a good fit. Such a variation in our parameters from the global fit to the CD difference spectra can be rationalized by considering that within the B-state inhomogeneous distribution there may be a variation of photoconversion efficiencies (see the section Widths of the A- and B-States). This may lead to slight variations in the positions and widths of the features in the photoconversion difference spectra that are obtained using different illumination fluences.

The value of $f = -1.3 \pm 0.7$ suggests that a simple exciton dimer representation of these two states may be inadequate. The magnitude of f is consistent with the major exciton interaction being dimeric; however, other interactions are probably significant. Nonresonant interactions (between Q_y and Q_x) of a dimer (*64*, *65*) cannot provide an explanation for a nonunity f-value because the Q_x region displays no significant CD signal (data not shown), and the entire Q_y region is conservative.

The third component [(3) in Table 1] in the fit is at 14780 ± 10 cm^{-1} (676.6 ± 0.5 nm) with fwhm = 180 ± 15 cm^{-1} and most likely represents a higher energy state of the exciton system associated with the two sharp bands 1 and 2. Alternatively, it could represent intensity due to coupling of the electronic transition to a relatively high-frequency phonon mode (∼100−130 cm^{-1}), as recently suggested for a water-soluble single-Chl-binding protein (*60*). We consider this unlikely in the present work, as this vibrational transition would need to have a different polarization compared to the electronic origin upon which it is built in order to explain the CD spectrum. This could not occur for a phonon mode coupled in the usual Franck−Condon manner to the electronic transition. Band 1 found in the global fit to the CD difference spectra (682.7 ± 2.5 nm, fwhm = 70 ± 15 cm^{-1}) is associated with the B-state assigned by Jankowiak et al. (*45*) (683.0 nm, fwhm = 45 cm^{-1}). The differences in the widths seen between our work and the previous assignment by Jankowiak et al. (*45*) are addressed in a following section.

For an isolated band, the rotational strength can be determined by integration of the CD spectrum (*66*):

$$R = 0.247 \int \Delta\epsilon/\nu \, d\nu \qquad (1)$$

where R is the rotational strength in Debye−Bohr magneton, $\Delta\epsilon$ is the difference absorption extinction coefficient (M^{-1} cm^{-1}), and ν is energy (cm^{-1}). The magnitude of the rotational strength for the individual bands determined from the Gaussian fit to the CD difference spectra is larger than the CD attributable to monomeric Chl *a* (*60*, *61*). As an example, for trace d in Figures 1, 6, and 7, the area of the absorption bleach (∼683 nm feature) corresponds to ∼0.1 Chl *a* while the rotational strengths for the bands 1−3 (trace d, Figures 6 and 7) are +1.2, −1.5, and −0.3 Debye−Bohr magneton, respectively. The rotational strength for monomeric Chl *a* is in the range −0.08 to −0.094 Debye−Bohr magneton (*60*, *61*). This shows that the features in the CD difference spectrum cannot readily be attributed to the intrinsic monomeric CD of Chl *a*.

Pigment−protein interactions (*64*) might contribute to significant variations from a nominal monomeric magnitude of Chl *a* CD. However, to our knowledge no satisfactory theoretical or phenomenological description of such changes exists. We recently studied (*60*) a system that binds only two Chl *a* molecules in a well-defined native protein environment and found that the intrinsic monomeric CD was not altered significantly from its value in ether. This result provides support for the suggestion that exciton coupling is responsible for the CD of the long-wavelength Chl *a* of CP43 and that the photoconversion process results in disruption of this exciton coupling.

In the Results section we established that photoconversion of the (broad) A-state that is less efficient than for the (narrow) B-state, in agreement with Jankowiak et al. (*45*). In our attempts to fit the long-wavelength portion of our photoconversion absorption difference spectra, we found an increasing contribution from the A-state (683.0 ± 0.3 nm, fwhm = 170 ± 30 cm^{-1}) as a function of illumination fluence (Figure 1), relative to the B-state. For illumination fluences >200 J/cm^2 the relative areas of the A- and B-states were comparable. The B-state position and width correspond to band 1 in Table 1 from the global fit to the CD difference spectrum, and the A-state is band 4. The discrepancy in the width of the A-state assigned by Jankowiak et al. (*45*) (fwhm = 120 cm^{-1}) and our finding (170 ± 30 cm^{-1}) is addressed in a following section.

Absorption Strengths of the Long-Wavelength States. In this section we address the question of how to accommodate the four long-wavelength states we have identified through CD and photoconversion data to the absorption spectrum of CP43. The contribution of these states to the structure near 683 nm in CP43 is significant as the prominent feature at ~683.5 nm in PSII core complexes isolated from spinach has been associated with P680 as well as CP43 (*4*, *14*, *32*, *48*, *49*, *67*−*70*). Previously (*47*, *71*) this feature was attributed entirely to CP43.

Attempts to fit the absorption, CD, or absorption difference spectra with an arbitrary number of Gaussian bands were not meaningful. The correlation matrix for such fits revealed that many of the parameters were strongly correlated. Our approach is to use the four bands identified from the photoconversion difference spectra (Table 1) as a minimal description for the long-wavelength region of the absorption spectrum. This procedure provides an *upper* limit for the absorption intensity that may be assigned to these bands, since it does not account for absorption intensity in this region due to the tail of bands from states at higher energy or other bands present. We limit our approach to the use of Gaussians to describe the shape of the individual absorption bands. Another approach might use a more general description of the band shape (*72*, *73*) or spectral broadening effects that are due to interacting pigments, where the band shape in CD may be expected to be narrower than in absorption (*74*).

The long-wavelength region of the CP43 absorption spectrum can be described well with the four states assigned from the photoconversion difference spectra when we let the positions and widths vary only within the error values (Table 1). The A-state at 683.0 ± 0.3 nm (fwhm = 170 ± 30 cm^{-1}) must be included to account for the absorption at wavelengths longer than 686 nm. The width of this state cannot be constrained to the value used by Jankowiak et al. (*45*) (i.e., 120 cm^{-1}) and still provide a good description of the absorption at wavelengths longer than 686 nm.

It is not possible to constrain the areas of each Gaussian to be equivalent to 1 Chl *a* and reproduce the long-wavelength region of the absorption spectrum. If the *sum* of the areas for the bands 1−3 is constrained to equal 3 Chl *a*, and the area of the A-state is not constrained, the long-wavelength absorption region is described well. The result of this fit is shown in Figure 8.

The constraint that the sum of the areas for bands 1−3 is equal to 3 Chl *a* is consistent with these bands being the components of an exciton-coupled system, as determined from the CD difference spectrum. The area of the A-state (band 4 in Figure 8) is less than 1 Chl *a*. This is consistent with the interpretation (*45*, *47*) that it is coupled excitonically to other Chl *a*, since this provides a mechanism for intensity redistribution to other states. Alternatively, our use of Gaussian band shapes rather than a full electronic-vibrational profile (*60*, *72*, *73*) may explain why an intensity of <1 Chl *a* is obtained. Jankowiak et al. (*45*) also suggested a similar explanation. Jankowiak et al. (*45*) estimated that the combined contribution of the A- and B-states was 1.7 ± 0.2 Chl *a*, in full agreement with our present analysis.

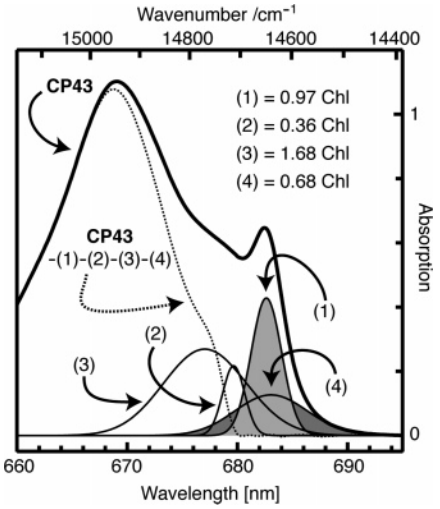

FIGURE 8: Fit of the long-wavelength part of the 1.7 K CP43 absorption spectrum that uses Gaussian bands and the positions and widths from Table 1 (see text for details). Bands 1 and 4 are associated with the B- and A-states assigned by Jankowiak et al. (*45*). Residual absorption in CP43 after subtraction of the four long-wavelength states is shown by the dotted line.

Widths of the A- and B-States. Jankowiak et al. (*45*) found the width of the A-state to be 120 cm^{-1} based on an analysis of the T − S spectra. These triplet bleaches were argued to be entirely due to the A-state. However, using the widths and positions of the A- and B-states in Table 1, we were able to fit the T − S data in Figure 3 of Jankowiak et al. (*45*) quantitatively with a ~25% contribution from the B-state (see Supporting Information). Groot et al. (*47*) have reported that the long-wavelength Chl *a* of CP43 have triplet lifetimes of ~0.6 and ~2.7 ms. A 25% contribution of the B-state to the T − S spectra is consistent with the B-state having the shorter lifetime.

The width of the B-state was measured to be 45 cm^{-1} by Jankowiak et al. (*45*) from the width of the depletion feature at ~683 nm after illumination at low fluence. We have assigned the width of the B-state as 70 ± 15 cm^{-1} from the fit of spectral changes obtained after high fluence illumination. The data in Figure 2 show that the width of the depletion taken at low fluences is ~45 cm^{-1}, in full agreement with the data of Jankowiak et al. (*45*). We suggest that the Chls with higher photoconversion efficiencies, and thus selectively photoconverted at lower fluences, have their B-state excitation energies in a narrower distribution compared to the full inhomogeneous spread of the B-state. The peaks of the high- and low-fluence depletions are also at slightly different energies, with the more efficient distribution peaking 0.3 nm to shorter wavelengths (Figure 2).

Special Photoconversion Mechanism in CP43. NPHB has characteristic thermal stabilities, quantum efficiencies, and dispersive kinetics (*58*). NPHB requires the selection of a subset of an inhomogeneous distribution of chromophores by a narrow-band excitation source, such as a laser. The mechanism involves subsequent tunneling in the excited state of the chromophore to an alternate configuration of the host (e.g., the glass or protein), which results in a change in the transition energy and therefore depletion in absorption at the excitation wavelength (i.e., a spectral hole). The photoproduct in NPHB lies within the inhomogeneous distribution of the system. The thermal stabilities, quantum efficiencies, and dispersive kinetics of the non-wavelength-selective photoconversion evident in CP43 are similar to those found for NPHB, but the photoproduct lies *well outside* the inhomogeneous distribution. This unusual characteristic requires a special mechanism for this photoconversion in CP43.

We propose a mechanism for the non-wavelength-selective photoconversion process involving quantum mechanical tunneling between alternate configurations that differ in the hydrogen bonding between protein residues and the Chl undergoing excitation. The archetypal mechanism for NPHB of chromophores in amorphous hosts involves small changes of the excitation energy of the chomophore due to tunneling of the host (glass) within two-level systems (TLSs) (*52*, *54*, *57*−*59*, *75*).

We have previously suggested (*46*) a mechanism for photoconversion in CP43 involving Chl−protein tautomerization that, for example, disrupts hydrogen bonding, and we expand on this suggestion here. The FLN spectra of Groot et al. (*47*) suggested the presence of strong hydrogen bonding of the Chl 13^1 C═O group of the sharp (B) state to the protein but weaker hydrogen bonding for the broader (A) state. Since photoconversion of the A-state has the lower efficiency, these FLN results are consistent with the association of hydrogen bonding with the photoconversion mechanism.

Hydrogen bonding of the Chl 13^1 C═O group to the protein in the B-state may explain its greater efficiency of photoconversion compared to the A-state. There will be a smaller barrier for quantum mechanical proton tunneling in a strong hydrogen bond, compared to a weak hydrogen bond. Photoconversion occurs via tunneling between alternate configurations of the C═O- - -H−protein hydrogen bond, when the molecule is in the excited electronic state. The thermal and temporal stability of the photoconverted state reflects the larger energy barrier in the ground state compared to the electronic excited state between the minima of the potential surfaces describing the hydrogen bond configurations.

The potential surface connecting two hydrogen bond configurations may be described as a TLS, and therefore our proposed mechanism bears analogy to the usual mechanism for NPHB of guest molecules in amorphous hosts. The distinction is that, for typical NPHB, the tunneling process involves TLS transitions of the host (*57*, *58*), whereas in our case the tunneling explicitly involves a guest−host (Chl−protein) rearrangement.

Host TLS tunneling, the usual mechanism for NPHB, is more efficient than the Chl−protein proton tunneling suggested for the special photoconversion process. NPHB dominates the difference spectra for narrow-band excitation that is resonant with the A- and B-states. Nonresonant excitation will induce NPHB processes, but these will have little consequence for the difference spectra as the photoproduct transition energies lie within the inhomogeneous distribution. The special photoconversion process, however, gives rise to a photoproduct lying *well outside* the inhomogeneous distribution, leading to a depletion of the A- and B-state absorptions.

Excitation Trapping in CP43. Jankowiak et al. (*45*) suggested that excitation energy is transferred primarily to the B-state. This assignment was based on the observation that the photoconversion efficiency of the B-state is much higher than that of the A-state and that since the A- and B-states have comparable NPHB efficiencies, the B-state received a greater proportion of excitation. In this work we have established that the photoconversion process that results in depletion of the absorption and CD spectra is *not* associated with the NPHB process. We have attributed the different photoconversion efficiencies for the A- and B-states to a mechanism distinct from that for NPHB. In this mechanism, photoconversion of the A-state is intrinsically less efficient than for the B-state.

Jankowiak et al. (*45*) have suggested that the B-state was responsible for most of the excitation energy transfer from CP43 to the reaction center of PSII and that the A-state played only a minor role. As excitation transfer among the Chl of isolated CP43 is much faster than fluorescence lifetimes (*38*), the lowest energy state will be responsible for fluorescence. The peak maxima of the A- and B-states are almost identical, with the A-state being significantly broader. Taking the energies of the A- and B-states to be uncorrelated, the lowest energy excitation in a collection CP43 particles will be on an A-state Chl in ∼50% of the sample and ∼50% on a B-state Chl. This is consistent with the analysis attributing comparable amounts of emission from both the A- and B-states (*47*). In light of this and our previous assignments (*14*, *28*, *32*, *48*, *49*), we suggest that both the A- and B-states in CP43 may be equally important for transferring excitation to the reaction center, and in oxygen-evolving PSII at low temperature they act as linker Chls.

CP43 Linkers in Oxygen-Evolving PSII. In this work we have studied the photophysical behavior of long-wavelength Chl *a* in isolated CP43 at low temperature. In oxygen-evolving PSII core complexes at low temperatures we have assigned these long-wavelength Chls as the linker molecules that connect this proximal antenna to the reaction center via energy transfer. In a PSII core complex, the energy-transfer times for these linkers are of the order ∼70 ps at 1.7 K in the "closed" ($S_1Q_A^-$) configuration (*14*, *32*) and most likely faster in the "open" (S_1Q_A) configuration (*14*). The photoconversion process in isolated CP43 occurs in the lowest electronic excited state of the long-wavelength Chl *a*. The radiative lifetime of this state is ∼8 ns (*45*). The efficiency of the photoconversion process of the low-energy CP43 Chl *a* states in PSII cores would then be expected to be lower by a factor of ∼100 (i.e., 8 ns/70 ps).

We performed experiments on PSII core complexes isolated from spinach to identify whether the photoconversion process seen in isolated CP43 also occurs for these low-energy Chls in a more intact assembly. No evidence for the occurrence of this photoconversion process in PSII core complexes was found (data not shown). However, in addition

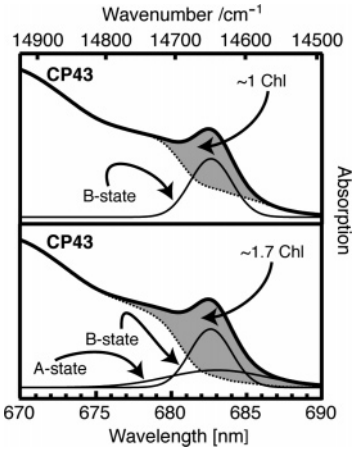

FIGURE 9: Our estimate for the maximum contribution of the A- and B-states to the 1.7 K CP43 absorption spectrum.

to the expected decrease in the efficiency of CP43 photoconverison (see above), such experiments are made difficult by far more efficient processes in PSII cores associated with photoinduced charge separation and reduction of the plastoquinone acceptor, Q_A^-. Formation of metastable Q_A^- having lifetimes from minutes to hours occurs with high initial efficiency of ~0.1−1 (*14*, *31*, *67*). This results in significant changes in the Chl absorption spectrum near ~683 nm associated with electrochromic shifts driven by the formation of Q_A^- and its partnering secondary donor (*14*, *67*). Whether the unique photoconversion process reported here is pathological and specific to isolated CP43 or whether it represents an inherent physiological flexibility of the Chl−protein interaction for the CP43 low-energy states remains an open question. If it is a distinct aspect of *isolated* CP43, it may reflect a change in the Chl−protein interaction and/or conformation as a consequence of the isolation procedure.

Given that the low-energy Chls in CP43 act as linkers even at the lowest temperature, they must be within immediate energy-transfer distance to the reaction center and are therefore most likely to be those that are the closest. Whether or not the low-energy CP43 Chls act as the linkers at physiological temperatures is still a matter of debate (*13*, *14*, *23*, *24*, *31*, *32*, *42*, *44*, *76*). In light of this, and with respect to our proposed photoconversion mechanism, it is therefore interesting that, of the three Chl *a* in CP43 [Chl41, Chl37, and Chl44 in the notation of Loll et al. (*10*)] that are closest to the reaction center pigments, only one is a likely candidate to be involved in hydrogen bonding of the 13^1 C═O group to the protein. From the 3.0 Å resolution crystal structure (*10*), the oxygen of the 13^1 C═O group of Chl41 is 4.0 Å from the phenolic oxygen atom of Tyr274. Investigation of the existence or absence of the photoconversion process in CP43 that has been isolated from cyanobacteria would provide a useful aid to identifying the linker Chls in the crystal structure.

There is a narrow, prominent absorption feature at ~683.5 nm in PSII cores prepared from spinach that carries the intensity of ~2 Chl *a* (*4*). This absorption feature has been attributed overlapping absorptions of a CP43 feature and a reaction center feature (*4*, *14*, *49*, *67*−*69*). In this work, we have addressed the contribution from the various long-wavelength states to the absorption in isolated CP43. Figure 9 (bottom panel) shows the relative contribution of the A- and B-states in the long-wavelength region. The combined contribution from both of these states is ~1.65 Chl *a* and represents the maximal absorption intensity attributable to the entire long-wavelength region. The contribution from the B-state alone is also presented (Figure 9, top panel). The area of the B-state corresponds to ~1 Chl *a*, consistent with our previous estimate for the maximum absorption intensity associated with the *sharp* 683 nm feature (*46*).

Thus, assuming that the absorption spectrum of CP43 does not change significantly upon its removal from the PSII core, only half of the absorption intensity of the ~683.5 nm feature in spinach PSII core complexes can be accounted for by CP43. The assumption that the CP43 spectrum does not change significantly may be reasonable, given that it is the most easily removed subunit of the PSII core complex (see refs *11* and *20* and references cited therein), and it is also the only subunit that retains a sharp absorption feature (at low temperature) following its isolation from the core (*68*).

Exciton Coupling and the CP43 Long-Wavelength Chl a States. In this section we discuss the exciton coupling that may give rise to the observed long-wavelength states that we have assigned. We do not present a detailed exciton calculation, since this is beyond the scope of this report.

Our photoconversion CD difference spectra establish that the B-state is the lowest energy component of an exciton-coupled system that cannot be adequately described as a dimer of equivalent Chls. From the CD difference spectra we identified three exciton states in this system (bands 1, 2, and 3 in Table 1), which establishes that there are at least three Chl *a* that contribute to this three-state exciton manifold. An intensity of less than 1 Chl *a* (Figure 8) for the A-state implies that it is a component of an exciton-coupled system, although we have not identified its exciton partners in our photoconversion difference spectra.

Changes in the absorption and CD spectra after photoconversion are due to modification of the monomeric Q_y transition energy of the Chl(s) contributing to the A- and B-states. After photoconversion at 1.7 K the relative orientations of the CP43 Chl *a* are unlikely to have changed. As a consequence, within the dipole−dipole approximation, the exciton coupling between any CP43 Chl *a* will not change after photoconversion, since the Chl *a* transition dipoles can be considered molecule-fixed. The effect of the coupling on the exciton transition energies is inversely proportional to the energy separation of the monomer transitions, with maximal exciton splitting occurring for degenerate monomers.

The B-state is mostly described as an excitation on a single Chl *a*. Following photoconversion, the absence of a clear absorption increase of a feature at wavelengths near the exciton partners of the B-state (bands 2 and 3, Table 1, Figure 8) suggests that the Chl contributing most significantly to the B-state must be only very weakly coupled to the other Chls within this three-state exciton manifold and/or has a significantly different monomeric transition energy. This means that the B-state arises due to an excitation predominantly localized on a single Chl *a*, consistent with our assignment of the absorption strength of ~1 Chl *a* to this state (Figure 8). The absorption intensities of bands 2 and 3 differ significantly from that of a single Chl *a* (Figure 8). This intensity redistribution is due to the effect of the exciton coupling of the Chls that give rise to these bands. To obtain

the substantial CD signals observed and the relative absorption intensities of bands 2 and 3, there must be coupling between the other two Chls that contribute to the three-state exciton manifold. These two Chls must be nearly degenerate for the coupling to have any significant effect on the absorption/CD spectra. The energy separation of bands 2 and 3 determined from the CD difference spectrum is 110 ± 55 cm^{-1}. In the simplest description this would mean that the coupling energy is $\sim 55 \pm 28$ cm^{-1}.

The phenomenology associated with the three-state exciton manifold involves a nonexcitonically red-shifted (~683 nm) B-state Chl *a* that is weakly coupled to at least two other Chl *a*. The other (two) Chls must have a near degeneracy of their monomeric transitions. This assignment of weak coupling of the B-state Chl *a* to other Chls in CP43 is consistent with Jankowiak et al. (*45*) and Groot et al. (*47*). Our finding that the monomeric transition energy of the B-state Chl *a* is in the long-wavelength region (~683 nm) is consistent with the conclusion by de Weerd et al. (*38*) that the red shift of the Chl responsible for the sharp long-wavelength feature of the CP43 absorption spectrum is due to a nonexcitonic interaction.

Jankowiak et al. (*45*) and Groot et al. (*47*) have both assigned weak coupling of the long-wavelength Chl *a* to higher energy Q_y transitions. These assignments were based on bleaching in T − S and NPHB difference spectra at higher energy that was correlated with the bleaching of the long-wavelength state(s). Jankowiak et al. (*45*) assigned correlation of the A-state with a state(s) at ~669 nm and correlation of the B-state with states at ~678 and ~673 nm, respectively.

We see no clear evidence in our absorption difference spectra for a change at ~678 nm that could be associated with depletion of the B-state. We account for the photoproduct in our difference spectra quantitatively, and we also obtained photoconversion in the absence of narrow-band NPHB. We observed a minimum in the photoproduct distribution at ~673 nm (see Results, Figure 1) and suggested that this arose from two distinct photoproduct distributions peaking near ~668 and ~677 nm.

From their T − S spectra, Groot et al. (*47*) did not find any strong evidence for a higher energy exciton partner of the B-state. The resolution in their T − S spectra was 3 nm, which is comparable to the width of the B-state and the energy separation to its sharp higher energy partner. Exciton coupled state(s) at ~669 nm linked to the A-state have been assigned by both Jankowiak et al. (*45*) and Groot et al. (*47*). We are not able to confirm such a phenomenon, as photoproduct formation in this spectral region resulting from photoconversion of the A- and B-states would overlap with any such depletion.

CONCLUSION

Our absorption and CD photoconversion difference spectra have established four Chl states in the long-wavelength (low-energy) region of isolated CP43. We assigned the position and widths of these states and estimated their contribution to the absorption spectrum. The exciton coupling involved with these states is weak and determined from our optical spectra to be maximally of the order ~50 cm^{-1}. The two states at lowest energy (~683 nm) are the excitation energy traps in isolated CP43 and are each predominantly localized on a single Chl *a*, consistent with earlier reports (*38*, *45*, *47*). The two other states that we have assigned are associated with weak exciton coupling to the narrow (fwhm ~70 cm^{-1}) trap state (B-state, ~683 nm). We proposed a unique mechanism for photoconversion that involves Chl−protein hydrogen bonding. Whether the photophysical behavior of these low-energy Chl *a* in isolated CP43 is distinctly different from the behavior of these Chls in PSII core complexes remains an open question. Further studies to address this question and the proposed photoconversion mechanism may provide insight into the physiological flexibility of the Chl−protein interaction for the low-energy Chl states of CP43.

SUPPORTING INFORMATION AVAILABLE

Fit of the T − S spectra of Jankowiak et al. (*45*) using our widths for the A- and B-states. This material is available free of charge via the Internet at http://pubs.acs.org.

REFERENCES

1. Berthold, D. A., Babcock, G. T., and Yocum, C. F. (1981) A Highly Resolved, Oxygen-Evolving Photosystem II Preparation from Spinach Thylakoid Membranes. EPR and Electron-Transport Properties, *FEBS Lett. 134*, 231−234.
2. Nanba, O., and Satoh, K. (1987) Isolation of a Photosystem II Reaction Center Consisting of D-1 and D-2 Polypeptides and Cytochrome *b*-559, *Proc. Natl. Acad. Sci. U.S.A. 84*, 109−112.
3. Seibert, M. (1993) Biochemical, Biophysical, and Structural Characterization of the Isolated Photosystem II Reaction Center Complex, in *The Photosynthetic Reaction Center* (Deisenhofer, J., and Norris, J., Eds.) pp 319−356, Academic Press, New York.
4. Smith, P. J., Peterson, S., Masters, V. M., Wydrzynski, T., Styring, S., Krausz, E., and Pace, R. J. (2002) Magneto-Optical Measurements of the Pigments in Fully Active Photosystem II Core Complexes from Plants, *Biochemistry 41*, 1981−1989.
5. Zouni, A., Witt, H. T., Kern, J., Fromme, P., Krauss, N., Saenger, W., and Orth, P. (2001) Crystal Structure of Photosystem II from *Synechococcus elongatus* at 3.8 Å Resolution, *Nature 409*, 739−743.
6. Kamiya, N., and Shen, J.-R. (2003) Crystal Structure of Oxygen-Evolving Photosystem II from *Thermosynechococcus vulcanus* at 3.7-Å Resolution, *Proc. Natl. Acad. Sci. U.S.A. 100*, 98−103.
7. Kamiya, N., and Shen, J.-R. (2001) in *PS2001: 12th International Congress of Photosynthesis*, pp S5-002, Brisbane, Australia.
8. Ferreira, K. N., Iverson, T. M., Maghlaoui, K., Barber, J., and Iwata, S. (2004) Architecture of the Photosynthetic Oxygen-Evolving Center, *Science 303*, 1831−1838.
9. Biesiadka, J., Loll, B., Kern, J., Irrgang, K.-D., and Zouni, A. (2004) Crystal Structure of Cyanobacterial Photosystem II at 3.2 Å Resolution: A Closer Look at the Mn-Cluster, *Phys. Chem. Chem. Phys. 6*, 4733−4736.
10. Loll, B., Kern, J., Saenger, W., Zouni, A., and Biesiadka, J. (2005) Towards Complete Cofactor Arrangement in the 3.0 Å Resolution Crystal Structure of Photosystem II, *Nature 438*, 1040−1044.
11. Bricker, T. M., and Frankel, L. K. (2002) The Structure and Function of CP47 and CP43 in Photosystem II, *Photosynth. Res. 72*, 131−146.
12. Yoder, L. M., Cole, A. G., and Sension, R. J. (2002) Structure and Function in the Isolated Reaction Center Complex of Photosystem II: Energy and Charge-Transfer Dynamics and Mechanism, *Photosynth. Res. 72*, 147−158.
13. Prokhorenko, V. I., and Holzwarth, A. R. (2000) Primary Processes and Structure of the Photosystem II Reaction Center: A Photon Echo Study, *J. Phys. Chem. B 104*, 11563−11578.
14. Hughes, J. L., Prince, B. J., Krausz, E., Smith, P. J., Pace, R. J., and Riesen, H. (2004) Highly Efficient Spectral Hole-Burning in Oxygen-Evolving Photosystem II Preparations, *J. Phys. Chem. B 108*, 10428−10439.
15. Holzwarth, A. R. (1991) Excited-State Kinetics in Chlorophyll Systems and Its Relationship to the Functional Organization of the Photosystems, in *Chlorophylls* (Scheer, H., Ed.) pp 1125−1151, CRC Press, Boca Raton, FL.

16. Greenfield, S. R., and Wasielewski, M. R. (1996) Excitation Energy Transfer and Charge Separation in the Isolated Photosystem II Reaction Center, *Photosynth. Res. 48*, 83−97.
17. Greenfield, S. R., Seibert, M., and Wasielewski, M. R. (1999) Time-Resolved Absorption Changes of the Pheophytin Q_x Band in Isolated Photosystem II Reaction Centers at 7 K: Energy Transfer and Charge Separation, *J. Phys. Chem. B 103*, 8364−8374.
18. Dekker, J. P., and van Grondelle, R. (2000) Primary Charge Separation in Photosystem II, *Photosynth. Res. 63*, 195−208.
19. Loll, B., Kern, J., Zouni, A., Saenger, W., Biesiadka, J., and Irrgang, K.-D. (2005) The Antenna System of Photosystem II From *Thermosynechococcus elongatus* at 3.2 Å Resolution, *Photosynth. Res. 86*, 175−184.
20. Alfonso, M., Montoya, G., Cases, R., Rodríguez, R., and Picorel, R. (1994) Core Antenna Complexes, CP43 and CP47, of Higher Plant Photosystem II. Spectral Properties, Pigment Stoichiometry, and Amino Acid Composition, *Biochemistry 33*, 10494−10500.
21. Yakushevska, A. E., Keegstra, W., Boekema, E. J., Dekker, J. P., Andersson, J., Jansson, S., Ruban, A. V., and Horton, P. (2003) The Structure of Photosystem II in *Arabidopsis*: Localization of the CP26 and CP29 Antenna Complexes, *Biochemistry 42*, 608−613.
22. Boekema, E. J., van Roon, H., Calkoen, F., Bassi, R., and Dekker, J. P. (1999) Multiple Types of Association of Photosystem II and its Light-Harvesting Antenna in Partially Solubilized Photosystem II Membranes, *Biochemistry 38*, 2233−2239.
23. Miloslavina, Y., Szczepaniak, M., Müller, M. G., Sander, J., Nowaczyk, M., Rögner, M., and Holzwarth, A. R. (2006) Charge Separation Kinetics in Intact Photosystem II Core Particles Is Trap-Limited. A Picosecond Fluorescence Study, *Biochemistry 45*, 2436−2442.
24. Holzwarth, A. R., Mueller, M. G., Reus, M., Nowaczyk, M., Sander, J., and Roegner, M. (2006) Kinetics and Mechanism of Electron Transfer in Intact Photosystem II and in the Isolated Reaction Center: Pheophytin Is the Primary Electron Acceptor, *Proc. Natl. Acad. Sci. U.S.A. 103*, 6895−6900.
25. van Grondelle, R., Dekker, J. P., Gillbro, T., and Sundstrom, V. (1994) Energy Transfer and Trapping in Photosynthesis, *Biochim. Biophys. Acta 1187*, 1−65.
26. Schatz, G. H., Brock, H., and Holzwarth, A. R. (1988) Kinetic and Energetic Model for the Primary Processes in Photosystem II, *Biophys. J. 54*, 397−405.
27. Schatz, G. H., Brock, H., and Holzwarth, A. R. (1987) Picosecond Kinetics of Fluorescence and Absorbance Changes in Photosystem II Particles Excited at Low Photon Density, *Proc. Natl. Acad. Sci. U.S.A. 84*, 8414−8418.
28. Krausz, E., Hughes, J. L., Smith, P. J., Pace, R. J., and Peterson Årsköld, S. (2005) Assignment of the Low-Temperature Fluorescence in Oxygen-Evolving Photosystem II, *Photosynth. Res. 84*, 193−199.
29. Hughes, J. L., Smith, P. J., Pace, R. J., and Krausz, E. (2006) Spectral Hole-Burning at the Low-Energy Absorption Edge of Photosystem II Core Complexes, *J. Lumin. 119−120*, 298−303.
30. Hughes, J. L., Smith, P. J., Pace, R. J., and Krausz, E. (2006) Low Energy Absorption and Luminescence of Higher Plant Photosystem II Core Samples, *J. Lumin.* doi:10.1016/j.jlumin.2006.01.142.
31. Hughes, J. L., Smith, P., Pace, R., and Krausz, E. (2006) Charge Separation in Photosystem II Core Complexes Induced by 690−730 nm Excitation at 1.7 K, *Biochim. Biophys. Acta* doi:10.1016/j.bbabio.2006.05.035.
32. Hughes, J. L., Krausz, E., Smith, P. J., Pace, R. J., and Riesen, H. (2005) Probing The Lowest Energy Chlorophyll *a* States of Photosystem II via Selective Spectroscopy: New Insights on P680, *Photosynth. Res. 84*, 93−98.
33. Holzwarth, A. R., Müller, M. G., Gatzen, G., Hucke, M., and Griebenow, K. (1994) Ultrafast Spectroscopy of the Primary Electron and Energy Transfer Processes in the Reaction Center of Photosystem II, *J. Lumin. 60−61*, 497−502.
34. Groot, M. L., Dekker, J. P., van Grondelle, R., den Hartog, F. T. H., and Völker, S. (1996) Energy Transfer and Trapping in Isolated Photosystem II Reaction Centers of Green Plants at Low Temperature. A Study by Spectral Hole Burning, *J. Phys. Chem. 100*, 11488−11495.
35. Groot, M. L., Breton, J., van Wilderen, L. J. G. W., Dekker, J. P., and van Grondelle, R. (2004) Femtosecond Visible/Visible and Visible/Mid-IR Pump-Probe Study of the Photosystem II Core Antenna Complex CP47, *J. Phys. Chem. B 108*, 8001−8006.
36. Groot, M.-L., van Mourik, F., Eijckelhoff, C., van Stokkum, I. H. M., Dekker, J. P., and van Grondelle, R. (1997) Charge Separation in the Reaction Center of Photosystem II Studied as a Function of Temperature, *Proc. Natl. Acad. Sci. U.S.A. 94*, 4389−4394.
37. den Hartog, F. T. H., Dekker, J. P., van Grondelle, R., and Völker, S. (1998) Spectral Distributions of "Trap" Pigments in the RC, CP47, and CP47-RC Complexes of Photosystem II at Low Temperature: A Fluorescence Line-Narrowing and Hole-Burning Study, *J. Phys. Chem. B 102*, 11007−11016.
38. de Weerd, F. L., van Stokkum, I. H. M., van Amerongen, H., Dekker, J. P., and van Grondelle, R. (2002) Pathways for Energy Transfer in the Core Light-Harvesting Complexes CP43 and CP47 of Photosystem II, *Biophys. J. 82*, 1586−1597.
39. Andrizhiyevskaya, E. G., Frolov, D., van Grondelle, R., and Dekker, J. P. (2004) On the Role of the CP47 Core Antenna in the Energy Transfer and Trapping Dynamics of Photosystem II, *Phys. Chem. Chem. Phys. 6*, 4810−4819.
40. Andrizhiyevskaya, E. G., Chojnicka, A., Bautista, J. A., Diner, B. A., van Grondelle, R., and Dekker, J. P. (2005) Origin of the F685 and F695 Fluorescence in Photosystem II, *Photosynth. Res. 84*, 173−180.
41. van Mourik, F., Groot, M.-L., van Grondelle, R., Dekker, J. P., and van Stokkum, I. H. M. (2004) Global and Target Analysis of Fluorescence Measurements on Photosystem 2 Reaction Centers upon Red Excitation, *Phys. Chem. Chem. Phys. 6*, 4820−4824.
42. Novoderezhkin, V. L., Andrizhiyevskaya, E. G., Dekker, J. P., and van Grondelle, R. (2005) Pathways and Timescales of Primary Charge Separation in the Photosystem II Reaction Center as Resolved by a Simultaneous Fit of Time-Resolved Fluorescence and Transient Absorption, *Biophys. J. 89*, 1464−1481.
43. Roelofs, T. A., Kwa, S. L. S., van Grondelle, R., Dekker, J. P., and Holzwarth, A. R. (1993) Primary Processes and Structure of the Photosystem II Reaction Center: II. Low-Temperature Picosecond Flourescence Kinetics of a D_1-D_2-cyt-*b*-559 Reaction Center Complex Isolated by Short Triton Exposure, *Biochim. Biophys. Acta 1143*, 147−157.
44. Vasil'ev, S., Orth, P., Zouni, A., Owens, T. G., and Bruce, D. (2001) Excited-State Dynamics in Photosystem II: Insights From the X-ray Crystal Structure, *Proc. Natl. Acad. Sci. U.S.A. 98*, 8602−8607.
45. Jankowiak, R., Zazubovich, V., Rätsep, M., Matsuzaki, S., Alfonso, M., Picorel, R., Seibert, M., and Small, G. J. (2000) The CP43 Core Antenna Complex of Photosystem II Possesses Two Quasi-Degenerate and Weakly Coupled Q_y-Trap States, *J. Phys. Chem. B 104*, 11805−11815.
46. Hughes, J. L., Prince, B. J., Peterson Årsköld, S., Krausz, E., Pace, R. J., Picorel, R., and Seibert, M. (2004) Photo-Conversion of Chlorophylls in Higher-Plant CP43 Characterized by Persistent Spectral Hole-Burning at 1.7 K, *J. Lumin. 108*, 131−136.
47. Groot, M.-L., Frese, R. N., de Weerd, F. L., Bromek, K., and Pettersson, A. (1999) Spectroscopic Properties of the CP43 Core Antenna Protein of Photosystem II, *Biophys. J. 77*, 3328−3340.
48. Hughes, J. L., Prince, B. J., Årsköld, S. P., Smith, P. J., Pace, R. J., Riesen, H., and Krausz, E. (2004) The Native Reaction Centre of Photosystem II: A New Paradigm for P680, *Aust. J. Chem. 57*, 1179−1183.
49. Krausz, E., Hughes, J. L., Smith, P., Pace, R., and Årsköld, S. P. (2005) Oxygen-Evolving Photosysten II Core Complexes: A New Paradigm Based on the Spectral Identification of the Charge-Separating State, the Primary Acceptor and Assignment of Low-Temperature Fluorescence, *Photochem. Photobiol. Sci. 4*, 744−753.
50. Hughes, J. L., Krausz, E., Smith, P. J., and Pace, R. J. (2004) in *PS2004: 13th International Congress of Photosynthesis* (van der Est, A., and Bruce, D., Eds.) pp S6A-3, Montreal, Canada.
51. Chang, H. C., Jankowiak, R., Yocum, C. F., Picorel, R., Alfonso, M., Seibert, M., and Small, G. J. (1994) Exciton Level Structure and Dynamics in the CP47 Antenna Complex of Photosystem II, *J. Phys. Chem. 98*, 7717−7724.
52. Reinot, T., Zazubovich, V., Hayes, J. M., and Small, G. J. (2001) New Insights on Persistent Nonphotochemical Hole Burning and Its Application to Photosynthetic Complexes, *J. Phys. Chem. B 105*, 5083−5098.
53. Johnson, S. G., and Small, G. J. (1989) Spectral Hole Burning of a Strongly Exciton-Coupled Bacteriochlorophyll *a* Antenna Complex, *Chem. Phys. Lett. 155*, 371−375.
54. Reddy, N. R. S., Lyle, P. A., and Small, G. J. (1992) Applications of Spectral Hole Burning Spectroscopies to Antenna and Reaction Center Complexes, *Photosynth. Res. 31*, 167−194.

55. Stranger, R., Dubicki, L., and Krausz, E. (1996) Magneto-Optical Investigation of the Exchange-Coupled Dimer $Cs_3Mo_2Br_9$, *Inorg. Chem. 35*, 4218−4226.
56. Riesen, H., and Hughes, J. L. (2003) Massive Enhancement of Persistent Spectral Hole-Burning in the R-lines of $NaMgAl(oxalate)_3 \cdot 9H_2O$:Cr(III) by Partial Deuteration, *Chem. Phys. Lett. 372*, 563−568.
57. Völker, S. (1989) Spectral Hole-Burning in Crystalline and Amorphous Organic Solids. Optical Relaxation Processes at Low Temperature, in *Relaxation Processes in Molecular Excited States* (Fünfschilling, J., Ed.) pp 113−242, Kluwer Academic Publishers, Dordrecht, Boston, and London.
58. Moerner, W. E., Ed. (1988) *Persistent Spectral Hole-Burning: Science and Applications*, Springer-Verlag, Berlin and Heidelberg.
59. Gille, J. K., Small, G. J., and Golbeck, J. H. (1989) Nonphotochemical Hole Burning of the Native Antenna Complex of Photosystem I (PS1-200) *J. Phys. Chem. 93*, 1620−1627.
60. Hughes, J. L., Razeghifard, R., Logue, M., Oakley, A., Wydrzynski, T., and Krausz, E. (2006) Magneto-Optic Spectroscopy of a Protein Tetramer Binding Two Exciton-Coupled Chlorophylls, *J. Am. Chem. Soc. 128*, 3649−3658.
61. Houssier, C., and Sauer, K. (1970) Circular Dichriosm and Magnetic Circular Dichroism of the Chlorophyll and Protochlorophyll Pigments, *J. Am. Chem. Soc. 92*, 779−791.
62. Tinoco, I. (1963) The Exciton Contribtution to the Optical Rotation of Polymers, *Radiat. Res. 20*, 133−139.
63. Cantor, C. R., and Schimmel, P. R. (1980) *Biophysical Chemistry. Part II: Techniques for the Study of Biological Structure and Function*, W. H. Freeman, San Francisco.
64. Mar, T., and Gingras, G. (1995) Origin of Optical Activity in the Purple Bacterial Reaction Center, *Biochemistry 34*, 9071−9078.
65. Koolhaas, M. H. C., van der Zwan, G., van Mourik, F., and van Grondelle, R. (1997) Spectroscopy and Structure of Bacteriochlorophyll Dimers. I. Structural Consequences of Nonconservative Circular Dichroism Spectra, *Biophys. J. 72*, 1828−1841.
66. Pearlstein, R. M. (1991) Theoretical Interpretation of Antenna Spectra, in *Chlorophylls* (Scheer, H., Ed.) pp 1047−1078, CRC Press, Boca Raton, FL.
67. Peterson Årsköld, S., Masters, V. M., Prince, B. J., Smith, P. J., Pace, R. J., and Krausz, E. (2003) Optical Spectra of *Synechocystis* and Spinach Photosystem II Preparations: Identification of the D1-Pheophytin Energies and Stark Shifts, *J. Am. Chem. Soc. 125*, 13063−13074.
68. Peterson Årsköld, S., Prince, B. J., Krausz, E., Smith, P. J., Pace, R. J., Picorel, R., and Seibert, M. (2004) Low-Temperature Spectroscopy of Fully Active PSII Cores. Comparisons with CP43, CP47, D1/D2/cyt b_{559} Fragments, *J. Lumin. 108*, 97−100.
69. Årsköld, S. P., Smith, P. J., Shen, J.-R., Pace, R. J., and Krausz, E. (2005) Key Cofactors of Photosystem II Cores from Four Organisms Identified by 1.7-K Absorption, CD, and MCD, *Photosynth. Res. 84*, 309−316.
70. Carbonera, D., Giacometti, G., and Agostini, G. (1994) A Well Resolved ODMR Triplet Minus Singlet Spectrum of P680 from PSII Particles, *FEBS Lett. 343*, 200−204.
71. Breton, J., and Katoh, S. (1987) Orientation of the Pigments in Photosystem II: Low-Temperature Linear-Dichroism study of a Core Particle and of its Chlorophyll-Protein Subunits Isolated from *Synechococcus* sp., *Biochim. Biophys. Acta 892*, 99−107.
72. Renger, T., and Marcus, R. A. (2002) On the Relation of Protein Dynamics and Exciton Relaxation in Pigment−Protein Complexes: An Estimation of the Spectral Density and a Theory for the Calculation of Optical Spectra, *J. Chem. Phys. 116*, 9997−10019.
73. Zucchelli, G., Jennings, R. C., Garlaschi, F. M., Cinque, G., Bassi, R., and Cremonesi, O. (2002) The Calculated In Vitro and In Vivo Chlorophyll a Absorption Bandshape, *Biophys. J. 82*, 378−390.
74. Somsen, O. J. G., van Grondelle, R., and van Amerongen, H. (1996) Spectral Broadening of Interacting Pigments: Polarized Absorption by Photosynthetic Proteins, *Biophys. J. 71*, 1934−1951.
75. Jankowiak, R., Hayes, J. M., and Small, G. J. (1993) Spectral Hole-Burning Spectroscopy in Amorphous Molecular Solids and Proteins, *Chem. Rev. 93*, 1471−1502.
76. Vasil'ev, S., Shen, J.-R., Kamiya, N., and Bruce, D. (2004) The Orientations of Core Antenna Chlorophylls in Photosystem II Are Optimized to Maximize the Quantum Yield of Photosynthesis, *FEBS Lett. 561*, 111−116.

BI0614683